Journal of Catalysis **189,** 129–146 (2000)
doi:10.1006/jcat.1999.2698, available online at http://www.idealibrary.com on IDEAL®

Ab Initio Study of the H_2–H_2S/MoS_2 Gas–Solid Interface: The Nature of the Catalytically Active Sites

P. Raybaud,* J. Hafner,† G. Kresse,† S. Kasztelan,‡ and H. Toulhoat*

*Division Informatique Scientifique et Mathématiques Appliquées, Institut Français du Pétrole, 1-4 av. de Bois-Préau, 92852 Rueil-Malmaison, France; ‡Division Cinétique et Catalyse, Institut Français du Pétrole, 92852 Rueil-Malmaison, France; and †Institut für Materialphysik and Center for Computational Materials Science, Universität Wien, Sensengasse 8, A-1090 Wien, Austria

Received June 10, 1999; revised September 9, 1999; accepted September 28, 1999

Despite the intense research efforts directed toward understanding the microscopic mechanism of hydrodesulfurization reactions on transition-metal–sulfide catalysts, the nature of active sites remains an open question. Industrial catalysts are mostly based on supported highly dispersed MoS_2. There is a general agreement that the active centers are coordinatively unsaturated sites at the edge surfaces oriented parallel to the hexagonal axis of this layered sulfide, but the precise local structure is still unknown. In the present ab initio study, we show that the nature and the concentration of the active sites as well as the shape of the MoS_2 crystallite can vary with the chemical potentials in the reactive atmosphere above the surface. We also report a precise investigation of the surface structure, chemical composition, and electronic properties of the MoS_2 edge surface under working conditions.

Key Words: **hydrodesulfurization catalysts; molybdenum disulfide; surface structure; surface chemical composition; density functional calculations.**

INTRODUCTION

For many years MoS_2-based catalysts have been widely used in heterogeneous hydrodesulfurization (HDS) catalysis. It is well established from various experimental techniques such as TEM (1, 2) and XPS (3, 4) that under working conditions the active phase of these catalysts consists of nanosized patches of the MoS_2 layered structure. EXAFS (5–8) gives also insights on the local structure of the active phase. The geometrical model proposed by S. Kasztelan *et al.* (9) for unpromoted and promoted MoS_2 particles and other descriptive models for the surface active sites (10) suggested that the morphology and the structure effects determine to a significant extent the properties of supported hydrotreating catalysts.

Nevertheless many questions raised about the detailed mechanisms of this catalytis are still open. Theoretical studies started 15 years ago attempt to provide insights at a microscopic level. One of the first theoretical investigation has been carried out by Harris and Chianelli (11, 12) on transition metal sulfide (TMS) clusters using the SCF-X_α scattered wave method. These authors studied the periodic trends in the activies of TMS catalysts and proposed an interpretation in terms of the TMS *d*-band shift. Zonnevylle *et al.* (13), using the Extended Hückel method, studied the adsorption of thiophene on molybdenum edge sites of a periodic system representing MoS_2. They concluded that the coordinatively unsaturated metal atoms are the active sites and that the reactivity is enhanced by creating vacancies at the neighboring sulfur sites. Although these early studies have opened new ways of investigation, they suffered from limitations of the theoretical development and from the modest computational tools available at that time. Cluster models (11, 12) which represent the catalyst by a small group of atoms do not account with sufficient accuracy for the actual environment of the surface active site. Furthermore even studies on periodic models (13) did not take into consideration a possible reconstruction of the surface since at the level of theory used, the computation of the forces acting on the ions was not possible. Some interesting investigations have also been carried out through molecular mechanics modeling (14) of small MoS_2 slabs exhibiting a range of coordinative unsaturation for surface Mo ions.

More accurate theoretical tools have been offered by the implementation of the Density Functional Theory (DFT) under the Generalized Gradient Approximation (GGA) coupled with pseudopotential methods on highly powerful computers. Recent works (15–17) on TMS systems have shown that the newest theoretical developments enable one to handle more and more complex systems. In two previous theoretical studies (18, 19) we have investigated the structural and electronic properties of the (10$\bar{1}$0) surface (also defined as "Mo-edge plane") and (1010) surface (also called "S-edge plane") surfaces exposing coordinatively unsaturated rows of Mo and S atoms in alternating S–Mo–S sandwiches.

We have demonstrated that the surfaces produced by cleaving the crystal along either of these planes are stable and undergo only a modest relaxation, even if the

0021-9517/00 $35.00

crystal is heated up to about 700 K in a MD simulation. The S atoms exposed at the edge of every second S–Mo–S layer are shown to be chemically inert, while the Mo atoms exposed in the next sandwiches exhibit a high local electronic density of states prone to strongly interact with sorbates (18). A subsequent study (19) demonstrated that a S-containing molecule such as thiophene is strongly bound in a η_5-geometry at the Mo edge and activated with respect to both C–S bond breaking and reduction of the aromatic character of the thiophene ring. However, it has to be emphasized that these calculations refer to the relaxed as-cleaved surface which is not necessary representative of the actual S/Mo ratio at the surface that will be determined under the conditions prevailing in an HDS reactor.

The S/Mo ratio is indeed determined by the concentration of sulfur species (sulfhydryl groups, H_2S, or sulfur organic compounds) chemisorbed on the (10$\bar{1}$0) and (1$\bar{0}$10) planes of the MoS_2 crystallite. It is known from experiment that the activity of the catalyst is stongly correlated to the S/Mo ratio (20, 21). It is thus of paramount importance to understand the factors controlling this parameter, a task not beyond the reach of ab initio calculations. The sulfur coverage of the edge planes depends directly on the local surface sulfur–metal bond energy which can be calculated ab initio.

In the present work we study the adsorption of sulfur on the Mo-terminated edges and the formation of vacancies on the S-terminated edges. Our calculations are based on the same model that has been used in our previous studies of MoS_2 surfaces, exposing three Mo atoms in one sheet and six S atoms on the neighboring sheet within the surface cell (see Fig. 1). As up to two S atoms can be adsorbed per surface Mo atom, this means that the S coverage may be varied between 0 and 100% on both edges, by steps of about 17%. Smaller and smaller increments in the sulfur coverage could be accounted for by using larger and larger models, but at the expense of a rapidly rising cost of calculations with the number of non equivalent atoms in the unit cell. We perform a full structural relaxation of each of these models and determine the heat of adsorption/desorption of surface species as well as the reaction enthalpy for the dissociative adsorption of gas-phase H_2S. The relative stability of the surfaces as a function of the chemical potential is discussed. We are therefore able to determine the surface speciation at equilibrium as a function of temperature and the ratio P_{H_2S}/P_{H_2} corresponding to given experimental reaction conditions. The electronic structures for various type of sites are also examined.

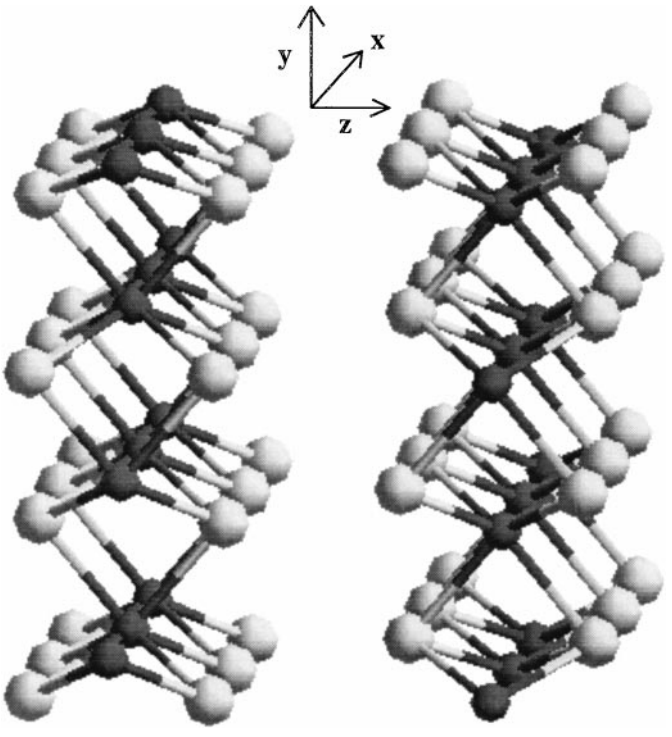

FIG. 1. Perspective view of the supercell used for modeling the MoS_2 edge surface after the low-temperature relaxation. This is defined as the stoichiometric as-cleaved surface with the bare Mo edge and the fully saturated S edge side. Small black balls, Mo atoms; large gray balls, S atoms.

METHOD

Our calculations are based on the density–functional theory, using the local exchange–correlation functional proposed by Perdew and Zunger (22), corrected for nonlocal effects thanks to the generalized gradient corrections developed by Perdew *et al.* (23). The surface is represented by a periodically repeated slab model, using a sufficiently thick vacuum layer to separate neighboring slabs. Electronic eigenstates are expanded in terms of plane waves, using pseudopotentials to describe the electron–ion interactions. Ultrasoft pseudopotentials (24–26) are particularly well suited to reducing the cutoff energy for the transition-metal pseudopotentials. The solution of the generalized Kohn–Sham equations valid for a system modeled by ultrasoft pseudopotentials is performed using the Vienna Ab-initio Simulation Package (VASP) (27, 28). VASP performs an iterative diagonalization of the Kohn–Sham Hamiltonian via unconstrained band-by-band minimization of the norm of the residual vector to each eigenstate and optimized charge density mixing routines. The optimization of the atomic geometry is performed using a conjugate gradient minimization of the total energy, using the exact Hellman–Feynman forces acting on the ions determined in each optimization step. For all technical details, including the construction of the ultrasoft pseudopotentials for Mo and S, we refer to our previous publications (18, 19). Hydrogen has also been modelled by an ultrasoft pseudotential for an atomic reference $1s^1 1p^0$. Cutoff radii for the pseudo-wavefunctions are $R_{c,s} = R_{c,p} = 0.66$ a.u. and the augmentation

radius for describing the localized part of the valence charge densities is $R_{aug,s} = 1.25$ a.u.

Our model for the MoS_2 surface is shown in Fig. 1. It consists of two S–Mo–S trilayers, stacked in the z direction. Each sandwich consists of three rows of MoS_6 prisms stacked in the y direction (plus rows of terminating Mo-atoms on one side of the slab) and three rows of prisms in the x direction. This 72-atom unit (composition $Mo_{24}S_{48}$) is periodically repeated in the x and z directions; in the y direction neighboring units are separated by a vacuum layer of 12.8 Å. All calculations have been performed at the equilibrium lattice constants of $a = 3.170$ (3.160) Å and $c = 12.584$ (12.294) Å calculated for bulk MoS_2 including generalized gradient corrections (15) (experimental lattice constants in parentheses). The space group of hexagonal MoS_2 is $P6_3/mmc$, TM atoms occupy the 2c positions with coordinates $(1/3, 1/3, 1/4 + z)$ (29). The theoretical equilibrium value is $z = 0.126$ (experiment $z = 0.119$). With these structural parameters, the ratio of the S–S distances across the trilayer and between different trilayers is 1.14 (experimental value 1.16). Hence the relative strength of the covalent bonding within the S–Mo–S sandwiches and of forces holding the sandwiches together is correctly described in the local-density approximation plus gradient corrections. Without the corrections the LDA underestimates the equilibrium volume by 6%, the GGC lead to an overestimate of 3%. The use of the GGCs is also mandatory for a correct description of the energetics of molecular adsorption at surfaces.

RESULTS

Energetics

Under reactive conditions, various sulfur containing molecules such as H_2S, thiophene, dibenzothiophene, and derivatives as well as H_2 are present. The surface sulfur coverage depends mainly on the chemical potential of these compounds in the gas phase. Within this study, we have chosen as a first step to evaluate the sulfur coverage at equilibrium. In this section we assume that equilibrium will correspond to the minimal enthalpy of reaction for the following process:

$$H_2(g) + (MoS_2 + S) \Leftrightarrow H_2S(g) + (MoS_2). \qquad [1]$$

Going from left to right corresponds to the desorption of a S atom from the surface and the formation of gas-phase H_2S with the reaction enthalpy:

$$\Delta E = E(H_2S) + E(MoS_2) - E(H_2) - E(MoS_2 + S). \quad [2]$$

The inverse reaction (right to left) corresponds to the dissociation of H_2S, the adsorption of a sulfur atom on the MoS_2 surface and the formation of molecular hydrogen in the gas phase. In this case, the heat of reaction is the same as given above, changing just the sign.

We must be aware that [1] is an idealized process since during the HDS reaction, it is well known that Mo–SH and eventually Mo–H surface groups are present so that the actual desorption process may be different from this model. Although the generation of an active site by desorption of S may involve not only the reaction of S with gas-phase hydrogen, but also the recombination of an adsorbed surface SH group with adsorbed atomic hydrogen or with another adsorbed SH group, we believe that reaction [1] should be a reliable guide for estimating the S coverage at equilibrium.

(i) Sulfur addition to the Mo-terminated edge. Our model consists of two MoS_2 sheets stacked in the z direction parallel to the hexagonal axis. Each sheet exhibits four MoS_2 layers in the y direction perpendicular to the surface. The periodicity in the x direction along the edges of the sheets is three Mo–Mo distances so that three inequivalent Mo surface sites are present. The initial stoichiometric slab corresponds to a S-free Mo edge and to a full coverage (100%) of the S edge (see Fig. 1). The Mo edge is fully saturated (100% coverage) when six sulfur atoms are added to the three coordinatively unsaturated sites (CUS) starting from the as-cleaved surface. The sulfur coverage on the Mo edge side is increased by adding sulfur atoms one by one, which corresponds to a sulfur coverage increase by step of 17% for each S added. The possible configurations are shown schematically in Fig. 2.

For a given coverage, it is required to determine the most stable configuration, i.e., the localization of the surface sulfur atoms leading to the lowest total energy. In Figs. 2a to 2g, schematic top views of the configurations for various sulfur coverages are represented. To make the vizualization easier, only one sheet and only the first outer surface layer is drawn. For the calculations, both sheets have been taken into account. We have added sulfur on both sides of the slab to form a symmetric model and to avoid the formation of an electrostatic field normal to the surface necessitating dipole corrections. The total energies are determined after a full ionic relaxation for the geometrical characterization of the relaxed surfaces (see section concerning the structural analysis). The total energy relative to the stoichiometric model used for the calculations of ΔE in Eq. [2] are reported in Fig. 2.

The reaction enthalpy for sulfur adsorption is plotted in Fig. 3 as a function of coverage (full line). The arrows show the energy cost (or gain) for removing one sulfur per Mo-edge surface or 17% of the sulfur atoms adsorbed at the Mo edge, via process [1], starting from a given sulfur coverage. The total energies of the H_2S and H_2 molecules calculated in the LDA + GGC are -6.74 and -11.06 eV, respectively (if isolated atoms are taken as reference). These values are used in Eq. [1].

On the Mo edge, the addition of S atoms is an exothermic process up to a sulfur coverage equal to 50%. A further increase of the sulfur coverage by 17% becomes unfavorable ($+0.46$ eV) and remains so up to 83%. From 83 to 100% the

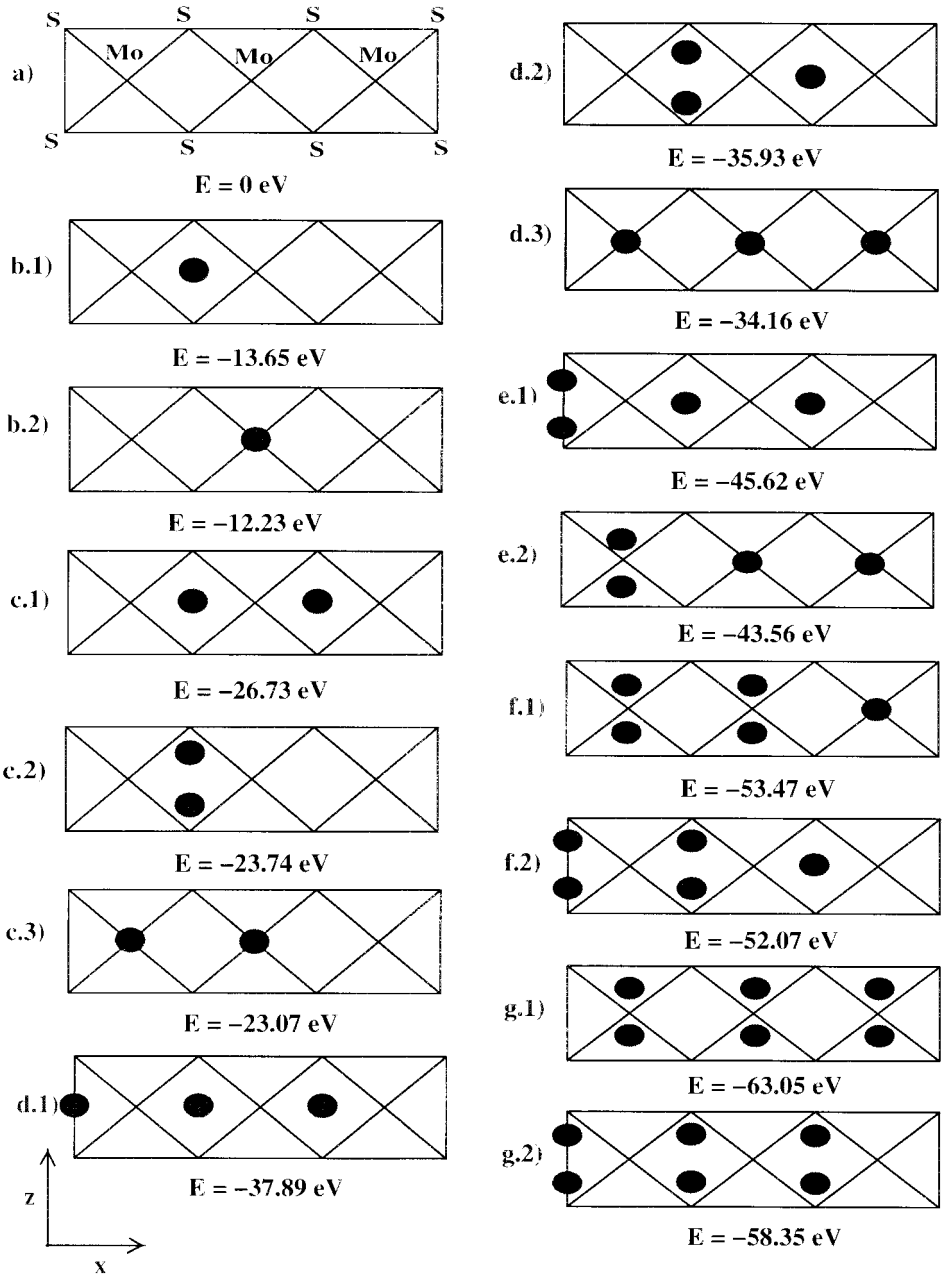

FIG. 2. Schematic top views of the Mo edge side with initial configurations for adsorbed sulfur atoms (dark circles). The sulfur coverages are for (a) 0%, (b) 17%, (c) 33%, (d) 50%, (e) 67%, (f) 83%, (g) 100%. For a given sulfur coverage, the configurations are numbered in the sequence of decreasing stability. Total energy values (eV/cell) after full relaxation are reported below each configuration. The energy reference (a) is the stoichiometric as-cleaved surface.

process is again exothermic but this coverage value is highly unlikely. The cost for removing 17% of sulfur atoms from a 50% coverage is about +1.26 eV. This result indicates that the surface has reached a state of minimal potential energy around the region of 50% sulfur coverage (see also section about the S coverage under varying chemical potential).

(ii) Formation of vacancies on the S-terminated edge. In the same way, we have investigated the gradual removal of S atoms from the S-terminated edge, beginning with the stoichiometric surface and ending with a full exposure of the underlying Mo atoms (see Figs. 1 and 4). For each S coverage, we have again performed a full structural optimization of several possible configurations. The relaxed geometries are compiled in Fig. 4 (for a detailed discussion of the surface structures, see below). From the total energies, we calculate again the heat of formation of an additional S vacancy, using Eq. [2].

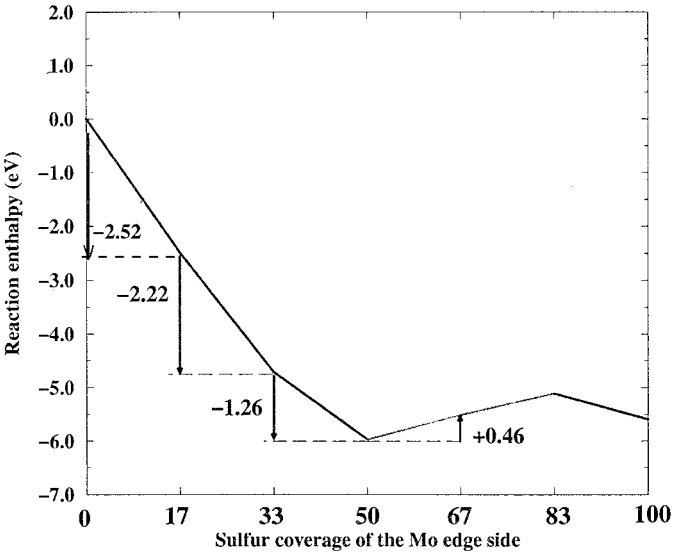

FIG. 3. Variation of the reaction enthalpy variation ΔE (in eV/atom) for sulfur adsorption as a function of the sulfur coverage (in percent) for the Mo edge side. The stoichiometric as-cleaved surface is the energy reference.

On the S edge, sulfur removal is always an endothermic process (see Fig. 5). Nevertheless we distinguish two main regions. At high sulfur coverage (>50%), the energy cost remains inferior to 1 eV/vacancy. At low sulfur coverage (<50%), sulfur removal becomes a highly endothermic process: the energy cost for removing 17% sulfur atoms is 1.87 eV/vacancy at 50% coverage and higher at lower coverage. Furthermore, the slab exhibits strong reconstructions after geometry optimization. This implies that under equilibrium conditions, the S coverage of the S-terminated edge can vary only between 100 and 50% (see also next section).

(iii) Sulfur exchange at fixed stoichiometry. So far, we have considered only the variation of the sulfur content on either the Mo- or S-terminated edge, with the chemical composition of the other edge fixed and corresponding to the as-cleaved surface. Assuming that sulfur addition on one edge and sulfur removal from the other edge are independent processes, we can consider the energetics of a sulfur exchange between both surfaces at a fixed total S coverage. For example, the heat of reaction for transfering one S atom from the fully covered S-terminated edge to the initially S-free Mo-terminated edge is approximated by the difference in the energies necessary to add one S atom to the Mo edge (the S edge remaining fully covered) and to remove one S atom from the S edge (without adding an atom to the Mo edge). This assumption has been checked by performing total energy calculations for the transfer of one S atom from the fully covered S edge to the bare Mo edge and found to be well satisfied (the difference in energy is smaller than 100 meV for the cases tested).

Figure 6 reports the variation of the total energy as a function of the distribution of the S atoms over the Mo- and S-terminated edges at various total S coverages (θ_S). The maximum coverage of $\theta_S = 100\%$ corresponds in our model to six S atoms on the Mo and on the S edges (i.e., altogether 12 S-surface atoms); $\theta_S = 50\%$ corresponds to the stoichiometric slab with six S surface atoms. The results for substoichiometric surfaces ($0\% < \theta_S \leq 50\%$) are shown in Fig. 6a as a function of the number of S atoms on the Mo edge, the reference being the S-free Mo-terminated edge. For the stoichiometric surface ($\theta_S = 50\%$), the striking result is that the total energy curve exhibits a minimum for a S coverage of 50% on both the Mo and the S edges (see also Fig. 6b). Starting from the as-cleaved surface, the transfer of up to three S atoms to the Mo edge and the creation of an equal number of vacancies on the S-terminated edge is an exothermic process, the energy gain being the largest if three S atoms are transferred. Even in the substoichiometric case, it is energetically favorable to distribute the S atoms over both edges as long as the total coverage exceeds $\theta_S = 25\%$. For the overstoichiometric case ($50\% \leq \theta_S < 100\%$), our results are shown in Fig. 6b as a function of the number of S atoms on the S edge, the reference energy being the fully covered S edge. Up to θ_S equal to 67%, the energetically most favorable distribution is achieved for a 50% coverage of the Mo-edge and the creation of the corresponding S vacancies on the S edge. Only for $\theta_S \geq 75\%$, the S edge remains always fully saturated.

S coverage under Varying Chemical Potential

Methods using the chemical potential and described in (i) were successfully applied to GaAs (30), c-BN (31, 32) and α-Fe_2O_3 (33) surfaces to determine the relative stabilities of different configurations at the surface. Furthermore, we make an attempt to give a detailed description in (ii) of the chemical potential of sulfur determined by the conditions (pressure and temperature) in gas phase.

(i) Definition and calculation of the grand potential, Ω, of the slab. So far we have considered only the energetics of S-adsorption and desorption from the MoS_2 surfaces without considering the chemical equilibrium between the surface and the reactive atmosphere containing essentially molecular hydrogen and H_2S.

In equilibrium, the S content of the MoS_2 surface is determined by the minimum of the grand potential, Ω, at temperature T, pressure p, and chemical potential of sulfur, μ_S, given by

$$\Omega = F(MoS_2 + n_S S) - \mu_S n_S = E(MoS_2 + n_S S) - TS - \mu_S n_S, \quad [3]$$

where F is the Helmoltz free energy of the slab, E the internal energy, and n_S sulfur atoms adsorbed or desorbed on the stoichiometric surface.

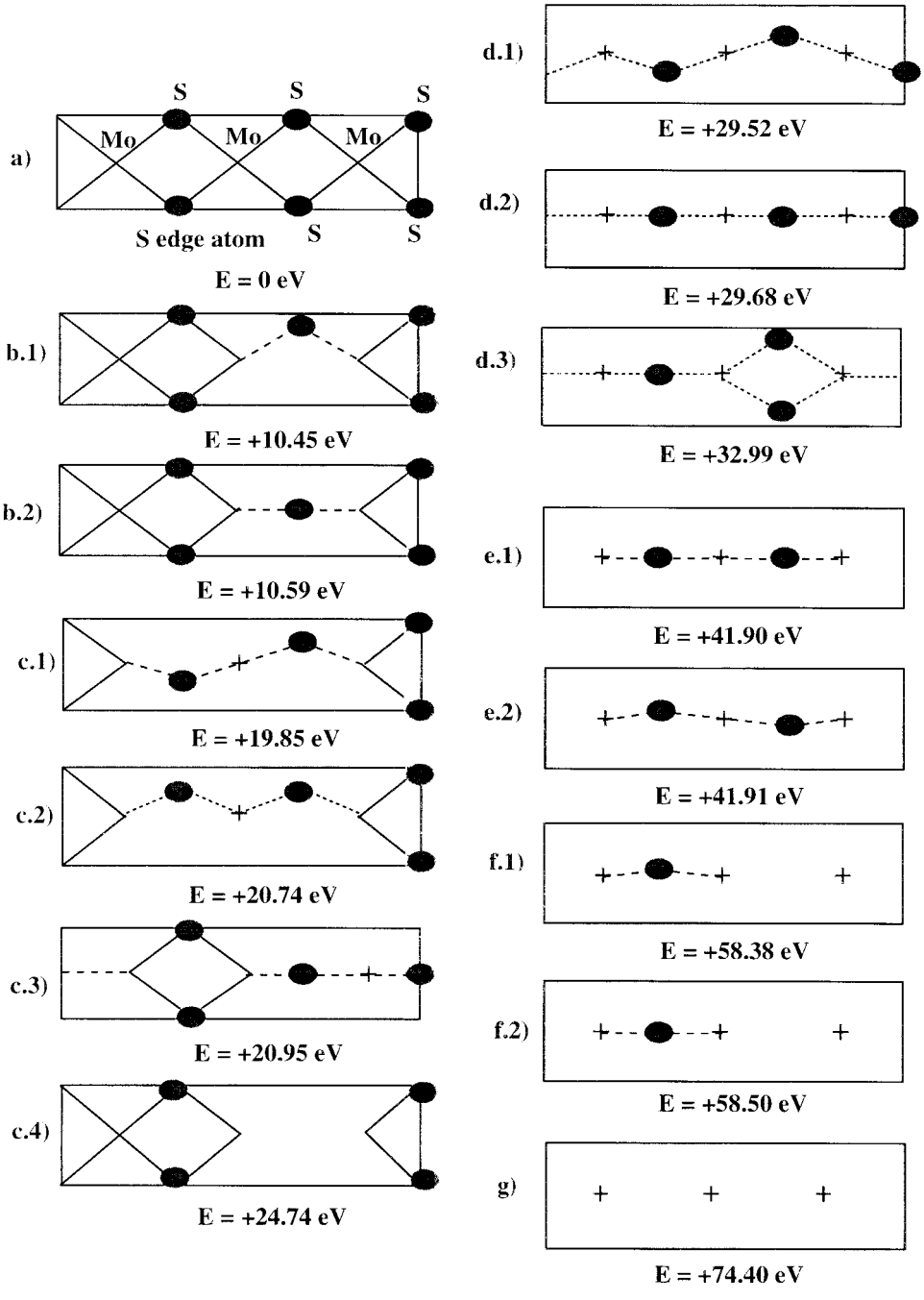

FIG. 4. Schematic top views of the S edge side with initial configurations for the terminal sulfur atoms (dark circles). The sulfur coverages are for (a) 100%, (b) 83%, (c) 67%, (d) 50%, (e) 33%, (f) 17%, (g) 0%. For a given sulfur coverage, the configurations are numbered in the sequence of decreasing stability. Total energy values (in eV/cell) after full relaxation are reported below each configuration. The energy reference (a) is the stoichiometric as-cleaved surface.

From the definition of Ω the reversible work for creating a small surface element, dA, at constant T, V, and μ, is given by

$$d\Omega = \sigma\, dA, \qquad [4]$$

where σ is the surface energy which depends on the surface orientation.

For the condensed states (as the MoS_2 surfaces, bulk MoS_2, Mo, and S), we neglect the the entropic terms. Within this approximation, the chemical potential of all condensed phases is set equal to the total energy E calculated at $T = 0$ K and the expression of the grand potential of the slab is

$$\Omega = E(MoS_2 + n_S S) - \mu_S n_S. \qquad [5]$$

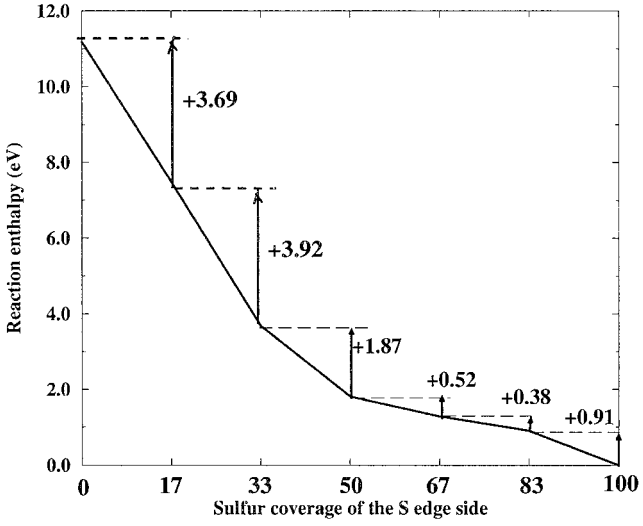

FIG. 5. Variation of the reaction enthalpy ΔE (in eV/atom) for the creation of sulfur vacancies as a function of the sulfur coverage (in percent) for the S edge side. The stoichiometric as-cleaved surface is the energy reference.

Ab initio calculations enable us to determine $E(MoS_2 + n_S S)$ for various n_S corresponding to the sulfur coverage varying between 0 and 100%. The variation of Ω as a function of the chemical potential μ_S is plotted for different S coverages of the MoS_2 surface in Fig. 7. According to Eq. [5] and for a given n_S, Ω varies linearly as a function of μ_S. The minimum of Ω at a fixed value of μ_S will give the stable state of the surface in terms of optimal n_S.

However, we have to remember that μ_S cannot take arbitrarily large values, but is determined by the chemical equilibrium between the surface and the gas phase. So the next step is to find how the variations of μ_S are connected with the conditions in the gas phase.

(ii) Evaluation of the chemical potential μ_S. At equilibrium, the chemical potential μ_S is the same in all the phases that are in contact and contain sulfur. At equilibrium between bulk MoS_2 and its components, the following relation holds:

$$\mu_{Mo} + 2\mu_S = \mu_{MoS_2(bulk)} \simeq E_{MoS_2(bulk)}. \quad [6]$$

The heat of formation of bulk MoS_2 is

$$\Delta H^f_{MoS_2} = E_{MoS_2(bulk)} - E_{Mo(bulk)} - 2E_{S(bulk)} \quad [7]$$

$$\simeq \mu_{MoS_2(bulk)} - \mu_{Mo(bulk)} - 2\mu_{S(bulk)}. \quad [8]$$

Combining Eqs. [6] and [8], we find that

$$\mu_S - \mu_{S(bulk)} \simeq +\frac{\Delta H_f}{2} - \frac{1}{2}[\mu_{Mo} - \mu_{Mo(bulk)}]. \quad [9]$$

The chemical potentials of Mo (μ_{Mo}) and of S (μ_S) have to remain smaller than the chemical potentials of bulk Mo ($\mu_{Mo(bulk)}$) and bulk S ($\mu_{S(bulk)}$), respectively, to avoid the decomposition of the MoS_2 catalyst. It follows from Eq. [9] that the chemical potential of sulfur can vary only within the boundaries

$$\frac{\Delta H_f}{2} \le \mu_S - \mu_{S(bulk)} \le 0, \quad [10]$$

where $\mu_{S(bulk)}$ is the chemical potential for the stable crystalline sulfur at low temperature, i.e., the orthorhombic S-alpha structure. Our calculations give $\mu_{S(bulk)} \simeq E_{S(bulk)} \simeq -4.02$ eV (-92.70 kcal/mol) after a relaxation of the atomic positions. The heat of formation ($\Delta H^f_{MoS_2}$) is estimated to be equal to -2.61 eV, i.e., -60.19 kcal/mol from our calculations. The experimental value given in (37) is -56.15 kcal/mol. Equation [10] leads to the following range of variation for μ_S (in eV):

$$-1.30 \le \mu_S - \mu_{S(bulk)} \le 0. \quad [11]$$

Furthermore the chemical potential of sulfur is determined by the chemical equilibrium with the gas-phase mixture ($H_2 + H_2S$), giving

$$\mu_S = \mu_{H_2S} - \mu_{H_2}. \quad [12]$$

For the gas phase, the temperature and pressure dependences of the chemical potential cannot be ignored. Assuming ideal gas-phase behavior and choosing the standard states ($T_0 = 298.15$ K, $p = 1$ atm) as references, for $\mu_S - \mu_{S(bulk)}$ we can derive

$$\mu_S - \mu_{S(bulk)} = \left[h_{H_2S}(T) - h_{H_2}(T)\right] - E_{S(bulk)} - T\left[s_{H_2S}(T) - s_{H_2}(T)\right] + RT \ln\left(\frac{p_{H_2S}}{p_{H_2}}\right), \quad [13]$$

where $h_{H_2S}(T)$ and $h_{H_2}(T)$ stand for the enthalpic contents and s_{H_2S} and s_{H_2} for the entropies at T for H_2S and H_2. (For improved accuracy, at high pressure the ratio of the partial pressures p_{H_2S}/p_{H_2} can be replaced by the ratio of fugacities.)

The first term in Eq. [13] can be expressed as follows:

$$\begin{aligned} h_{H_2S}(T) - h_{H_2}(T) - E_{S(bulk)} &= \left[h_{H_2S}(T) - h_{H_2S}(0)\right] - \left[h_{H_2}(T) - h_{H_2}(0)\right] \\ &+ \left[h_{H_2S}(0) - E_{H_2S}(0)\right] - \left[h_{H_2}(0) - E_{H_2}(0)\right] \\ &+ E_{H_2S}(0) - E_{H_2}(0) - E_{S(bulk)}. \end{aligned} \quad [14]$$

Our calculations give values for the internal energies of the free H_2 and H_2S molecules at $T = 0$ K leading to $E_{H_2S}(0) - E_{H_2}(0) - E_{S(bulk)} = -0.30$ eV (-5.1 kcal/mol). From the tabulated thermodynamic data (37), we can estimate that the change of μ_S due to the enthalpic term, $[h_{H_2S}(T) - h_{H_2S}(0)] - [h_{H_2}(T) - h_{H_2}(0)]$, for $T = 650$ K is $+0.04$ eV/atom, which represents a rather small contribution. The

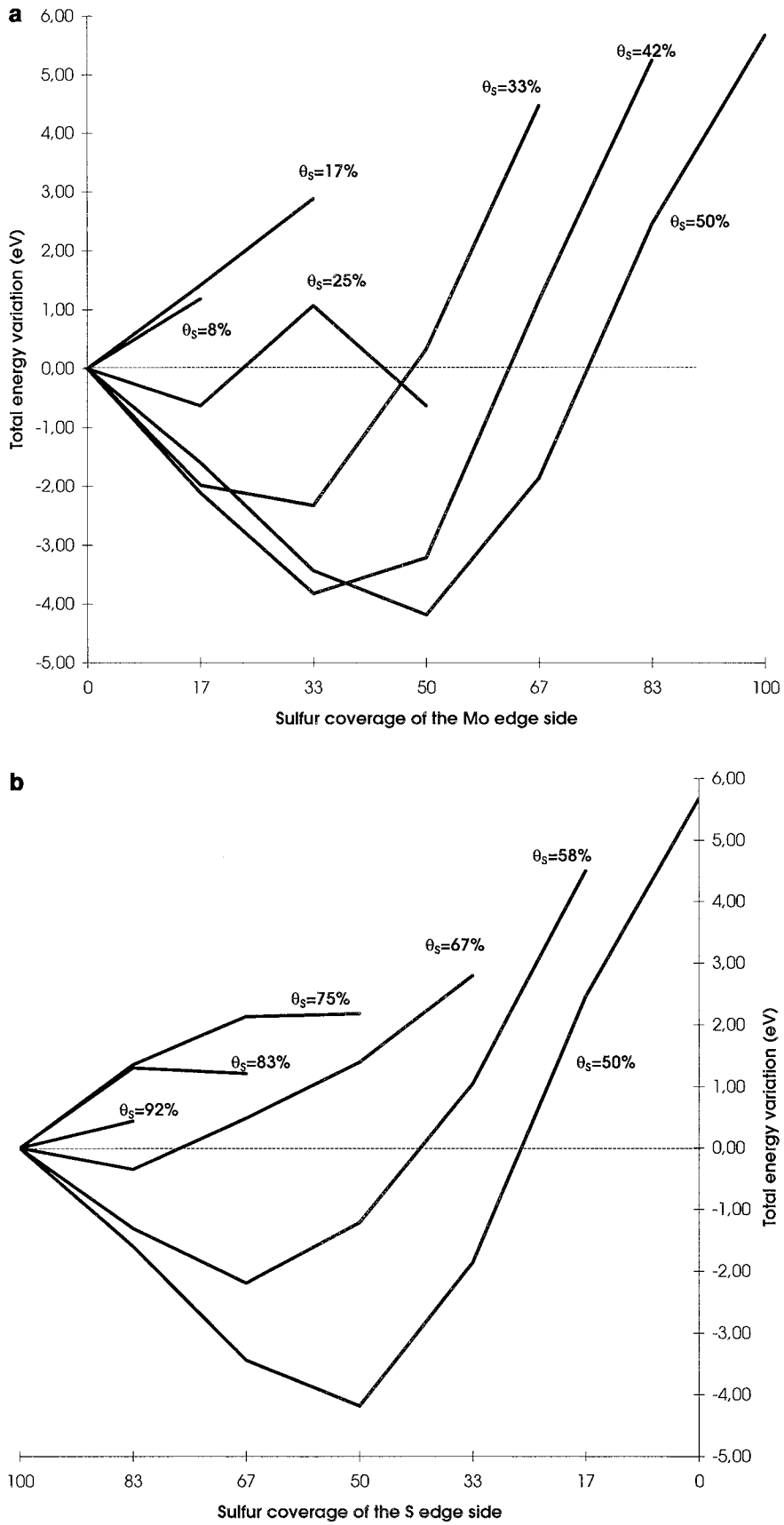

FIG. 6. Variation of the total energy (in eV/atom) of the slab as a function of the distribution of the S atoms over the Mo- and S-terminated edges, calculated for different total sulfur coverages (θ_S). $\theta_S = 100\%$ corresponds to a full saturation of both edges, corresponding in our model to six S atoms bound at each of the two edges, $\theta_S = 50\%$ to the stoichiometric surface. (a) The results for a substoichiometric surface ($\theta_S \leq 50\%$), the energy is plotted as a function of the S coverage of the Mo edge, the reference being the S-free Mo edge. (b) The results for the S-enriched surface ($50\% \leq \theta_S \leq 100\%$) as a function of the S coverage of the S edge, the reference being the fully saturated S edge (cf. text).

zero point vibrational energy term, $[h_{H_2S}(0) - E_{H_2S}(0)] - [h_{H_2}(0) - E_{H_2}(0)]$, is estimated at +0.12 eV through ab initio evaluation of normal mode frequencies. Altogether this leads to $[h_{H_2S}(T) - h_{H_2}(T)] - E_{S(bulk)} \simeq -0.14$ eV (−3.2 kcal/mol). For comparison, the tabulated thermodynamic data (37) yield $[h_{H_2S}(T) - h_{H_2}(T)] - E_{S(bulk)} = -0.19$ eV at $T = 650$ K. The remaining discrepancy is due to the fact that we have neglected the effect of temperature on the S-alpha phase (from 0 to 298.15 K) and to the difference in the measured and calculated enthalpies. To be consistent with the ab initio calculations of the energetics of the MoS_2 surfaces, the calculated value (−0.14 eV) must be used. It is marked by arrow 1 in Fig. 7.

The contribution of the entropic terms can be estimated directly from the thermodynamic data tables. It leads for $-T[s_{H_2S}(T) - s_{H_2}(T)] \simeq -0.58$ eV/atom (−13.4 kcal/mol) at $T = 650$ K, marked by arrow 2 in Fig. 7.

The pressure effect leads to a variation of μ_S between −0.1 eV/atom (−2.3 kcal/mol) and −0.25 eV/atom (−5.8 kcal/mol), if the ratio of p_{H_2S}/p_{H_2} varies between 0.10 and 0.01, respectively, for the given temperature $T = 650$ K. (Arrow 3 is marked for $p_{H_2S}/p_{H_2} = 0.01$ in Fig. 7).

(iii) Interpretation of the results. Figures 7a and 7b show the variation of the grand potential of the surface calculated for different S coverages on the Mo edge (a) or on the S edge (b) as a function of μ_S. The zero of the chemical potential of sulfur corresponds to the crystalline S-α structure.

The values of the grand potential are given relative to the relaxed stoichiometric, as-cleaved, surface, i.e., $\Omega = 0$ for $n_S = 0$. The lowest value of the grand potential at same μ_S gives the stable state of the surface for that particular chemical potential of sulfur. For the Mo edge (Fig. 7a), the important points are as follows: close to the maximum allowable value of the S-chemical potential (between −0.17 and 0 eV) a full S-coverage of the Mo edge is stable. However, for μ_S smaller than −0.17 eV and larger than −1.6 eV, a 50% coverage is stabilized. The reduction of μ_S induced by an increased temperature and a smaller ratio of p_{H_2S}/p_{H_2} further stabilizes a 50% coverage by S. We observe in agreement with the reaction enthalpies calculated in the previous section that a coverage greater than 50%, but strictly smaller than 100%, is unstable at any value of the S-chemical potential. We also note that within the accessible range of μ_S, the difference between 50 and 33% S coverage is small (and hence the appearance of coordinatively unsaturated surface Mo atoms is possible locally). The energy cost for creating such a surface sulfur vacancy for μ_S around −1.0 eV is about +0.5 eV (+11.5 kcal/mol). A small local fluctuation of the chemical potential could indeed induce this vacancy creation. Nevertheless, a S coverage lower than 50% of the Mo edge is stable only outside the physically realistic range of μ_S.

On the S-terminated edge (see Fig. 7b), the accessible range of μ_S includes the fully S-covered edge and the case of a reduced coverage of 50%—here again intermediate S coverages are not stabilized at any value of μ_S. The stability range of the fully covered S edge is sufficiently large so that the formation of S vacancies will occur only at extremely reduced values of μ_S. At realistic values of μ_S, characteristic for HDS conditions, the prediction is a 100% S coverage on the S-terminated edge and a 50% coverage on the Mo-terminated edge (assuming again that the variation of the S content on either edge can be treated as an independent process; cf. above).

However, the preceding analysis ignores the possibility of a S exchange between the Mo- and S-terminated edges. Assuming as in the previous section that the heat of reaction for a S exchange can be approximated in terms of the difference in the heats of desorption and adsorption, we can construct a generalized chemical potential diagram including also S-exchange processes. Figure 7c shows the variation of the grand potential for different S coverages of the (010) surface, taking into consideration simultaneously both Mo and S edges. For the allowed range of μ_S (between −1.30 and 0 eV/atom), the (010) surface can undergo surface phase transitions in two steps. Very close to $\mu_S = 0$, the fully saturated surface (100%, 100%) is the most stable. For conditions at which μ_S is smaller than −0.17 eV/atom and greater than −0.9 eV/atom, the stable surface corresponds to a fully saturated S edge and a 50% coverage of the Mo edge. If μ_S is further reduced (which is possible for T above 650 K and P_{H_2S}/P_{H_2} lower than 0.01) a (50%, 50%) coverage of the Mo and S edges can be reached (see Fig. 7c), but this corresponds to a highly reductive environment. The most realistic situation (corresponding to HDS conditions) leads to a fully saturated S edge and a 50% coverage of the Mo edge. This analysis is valid as long as the MoS_2 particle has a size sufficient in the a, b, and c directions so that van der Waals interactions stabilize the 2H structure and so that a (010) surface extended along the (001) direction can be defined.

(iv) Case of a single MoS_2 layer: Predictions of morphologies. In the case of highly dispersed particles on an oxide support (industrial working catalysts), where unstacked sheets containing a single MoS_2 layer are known to exist from TEM studies, we have to consider the Mo-terminated edge and the S-terminated edge as separate surfaces expressed in the particle morphology. The relevant energy diagrams should be Figs. 7a and 7b, respectively. However, these diagrams are constructed by using as energy reference the grand potential of the stoichiometric as-cleaved slab ($\Omega = 0$ for $n_S = 0$), and instead we require the absolute grand potentials of the Mo edge and of the S edge independently to estimate the surface energy of the Mo edge (σ_{Mo}) and of the S edge (σ_S). Such estimations will allow us to predict equilibrium morphologies of the nanosized

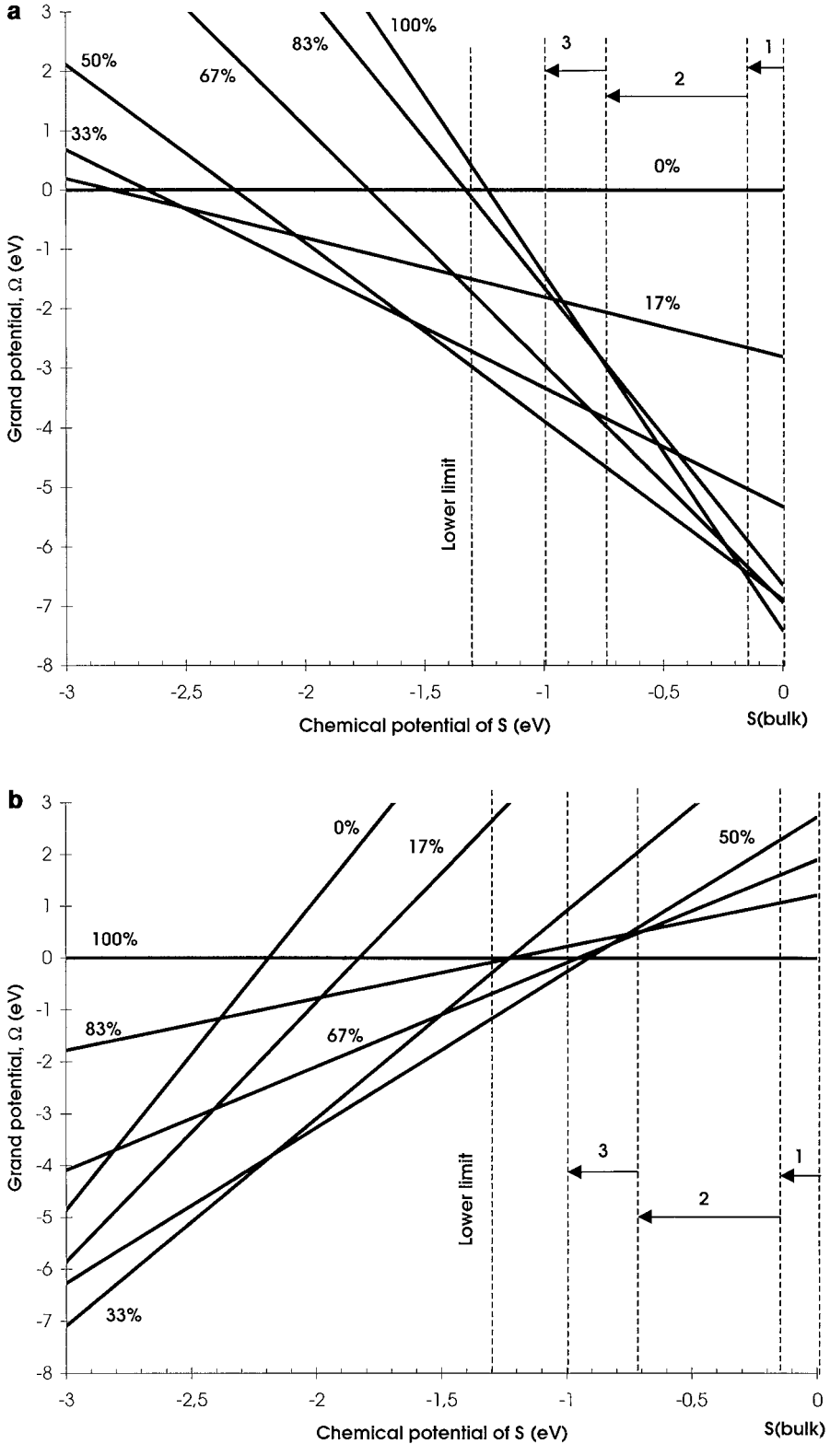

FIG. 7. Grand potential of the slab (in eV/atom) as a function of the chemical potential of S, μ_S (see Eq. [5]) on the Mo edge (a), S edge (b), and (010) surface (c). Each line corresponds to a given sulfur coverage (n_S fixed). For the (010) surface the notation (50%, 100%) corresponds to 50% coverage of the Mo edge and 100% of the S edge. The energy references for μ_S are the crystalline α-phase of S and the stoichiometric as-cleaved surface for the grand potential of the surface ($\Omega = 0$ for $n_S = 0$). Arrow 1 stands for the enthalpy contribution of H_2 and H_2S (calculated), arrow 2 for the entropy contribution, and arrow 3 for the pressure contribution (estimated as described in the text for $T = 650$ K and $p_{H_2S}/p_{H_2} = 0.01$).

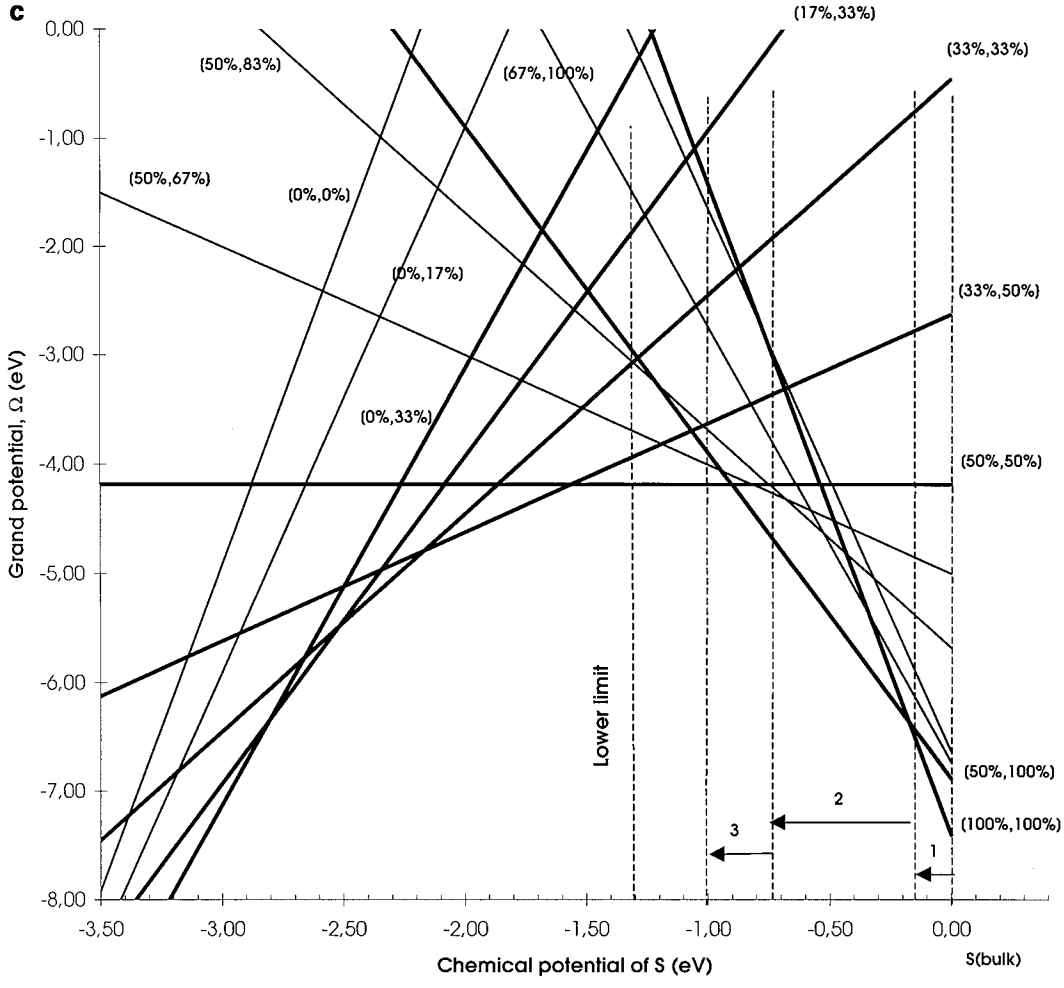

FIG. 7—*Continued*

MoS_2 sheets according to the Gibbs–Curie–Wulf construction. In our previous work (18) we have already determined the surface energy of the (010) surface as being equal to $\sigma_0 = 0.102$ eV Å^{-2}. We can write

$$\sigma_{Mo}^{0\%} + \sigma_S^{100\%} = 2\sigma_0, \qquad [15]$$

where $\sigma_{Mo}^{0\%}$ is the surface energy of the Mo-terminated edge with a 0% sulfur coverage, and $\sigma_S^{100\%}$ is the surface energy of the S-terminated edge with 100% of sulfur coverage.

We define k as the ratio of the surface energies,

$$k = \frac{\sigma_{Mo}}{\sigma_S}, \qquad [16]$$

where σ_{Mo} (resp. σ_S) is the surface energy of the Mo edge (resp. S edge) for a given μ_S.

For $k = 1$, both edges have the same surface energies and the shape of the MoS_2 crystallite is hexagonal, presenting the same areas for the three Mo edges and the three S edges. For $k < 1$ (resp. >1), the morphology of the particle is a deformed hexagon exhibiting the larger areas for the Mo edges (resp. S edges). For very small (resp. large) values of k, the shape tends toward the perfect triangle exhibiting three Mo edges (resp. S edges) only.

If we assume

$$\Delta\sigma_{Mo} = \sigma_{Mo} - \sigma_{Mo}^{0\%}, \qquad [17]$$

and

$$\Delta\sigma_S = \sigma_S - \sigma_S^{100\%}, \qquad [18]$$

$\Delta\sigma_{Mo}$ and $\Delta\sigma_S$ are directly connected to the variations of the grand potential plotted in Figs. 7a and 7b.

Combining Eqs. [15] to [18], we obtain the following expression:

$$\frac{\sigma_{Mo}^{0\%}}{\sigma_S^{100\%}} = \frac{2k\sigma_0 - \Delta\sigma_{Mo} + k\Delta\sigma_S}{2\sigma_0 + \Delta\sigma_{Mo} - k\Delta\sigma_S}. \qquad [19]$$

In Fig. 8, we have plotted the various domains of stability for the S edge and the Mo edge as a function of the chemical potential of S and of the ratio $\sigma_{Mo}^{0\%}/\sigma_S^{100\%}$. The vertical full lines are the boundaries of different chemical composition of a

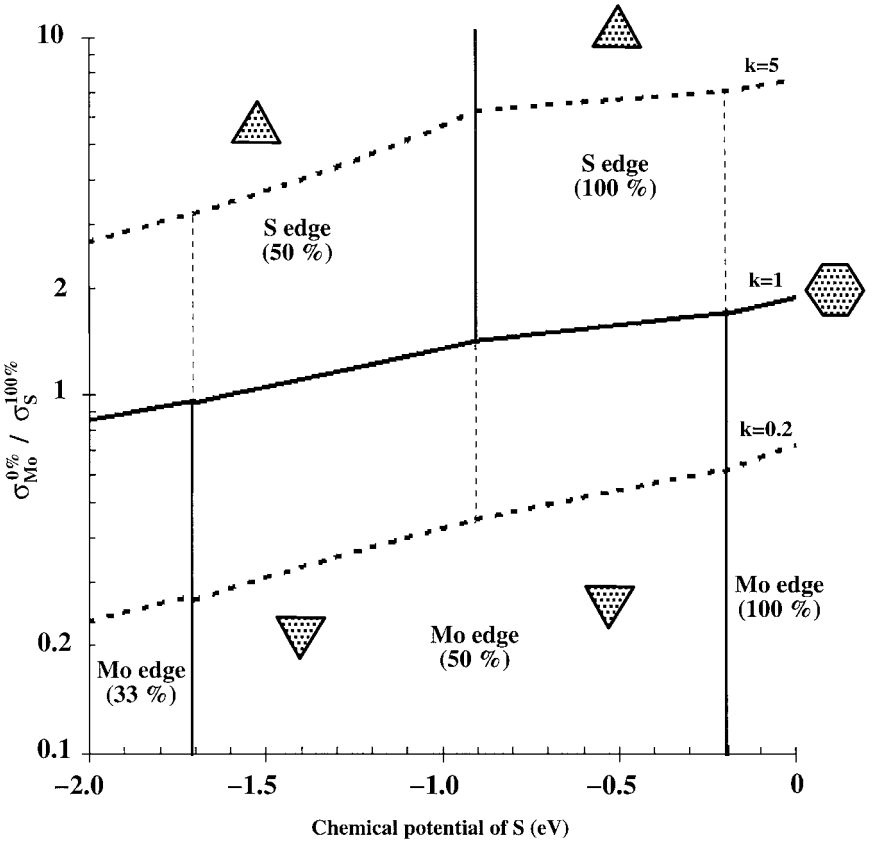

FIG. 8. Domains of stability of the Mo-terminated edge and S-terminated edge for the nonpromoted crystallite as a function of the chemical potential of sulfur (in eV) and of the ratio $\sigma_{Mo}^{0\%}/\sigma_{S}^{100\%}$ (in a logarithmic scale). The vertical straight lines are the boundaries of the different chemical compositions of the Mo edge and S edge. The curve in full lines ($k=1$) corresponds to the hexagonal morphology; curves in dashed lines ($k=0.2$ resp. $k=5$) correspond to a morphology very close to the triangle.

given edge. The full curve constructed for $k=1$ represents the values of $(\sigma_{Mo}^{0\%}/\sigma_{S}^{100\%}, \mu_S)$ for which the morphology is hexagonal. The dashed curve plotted for $k=0.2$ (resp. $k=5$) represents the values of $(\sigma_{Mo}^{0\%}/\sigma_{S}^{100\%}, \mu_S)$ for which the shape of the particule is a deformed hexagon very close to a triangle exhibiting preferentially the Mo edge (resp. S edge).

At this stage, it would be required to determine the precise value of the ratio $\sigma_{Mo}^{0\%}/\sigma_{S}^{100\%}$. However, we are not able to calculate the surface energies for the Mo-terminated edge and for the S-terminated edge independently. Indeed, the crystallographic plane of cleavage and the stacking sequence of the MoS_2 layers imply the simultaneous creation of Mo and S edges. For an evaluation of $\sigma_{Mo}^{0\%}$ and $\sigma_{S}^{100\%}$, it is required to simulate single-sheet crystallites with triangular shapes exhibiting only one kind of edge. This is beyond the scope of the present work. However, we can already underline the following important result: for a chemical potential of S varying roughly between −1.1 and −0.7 eV, and assuming a ratio $\sigma_{Mo}^{0\%}/\sigma_{S}^{100\%}$ around 1, we see that the crystallite may undergo "edge" phase transitions. The S edge/Mo edge transition will lead to shape transformations (variation of k) from a S edge triangle to a Mo edge triangle via deformed hexagons and perfect hexagonal crystallite where both Mo and S edges are present.

All these features could in principle be observed directly from high resolution STM studies under controlled atmosphere, in the same way as triangular morphologies have recently been reported [39].

Structural Analysis

(i) Mo-terminated edge surface. The calculation of the total energies has shown that the equilibrium sulfur coverage on the Mo-terminated edge is obtained for sixfold coordinated molybdenum atoms at the surface. The fully relaxed configurations of the Mo-terminated sheet are given in Fig. 9 for sulfur coverages of 50 and 33%, corresponding to the situations sketched in Figs. 2d1 and 2c1. For a 50% sulfur coverage, one sulfur atom per molybdenum atom is adsorbed on the surface in a bridging position (see Fig. 9a). The calculated Mo–Mo distances (3.17 to 3.22 Å) are in nice agreement with EXAFS data (5–8) which evaluate Mo–Mo distances close to the bulk Mo–Mo distance (3.16 Å). In the x direction, along the edge, the Mo–Mo distances are

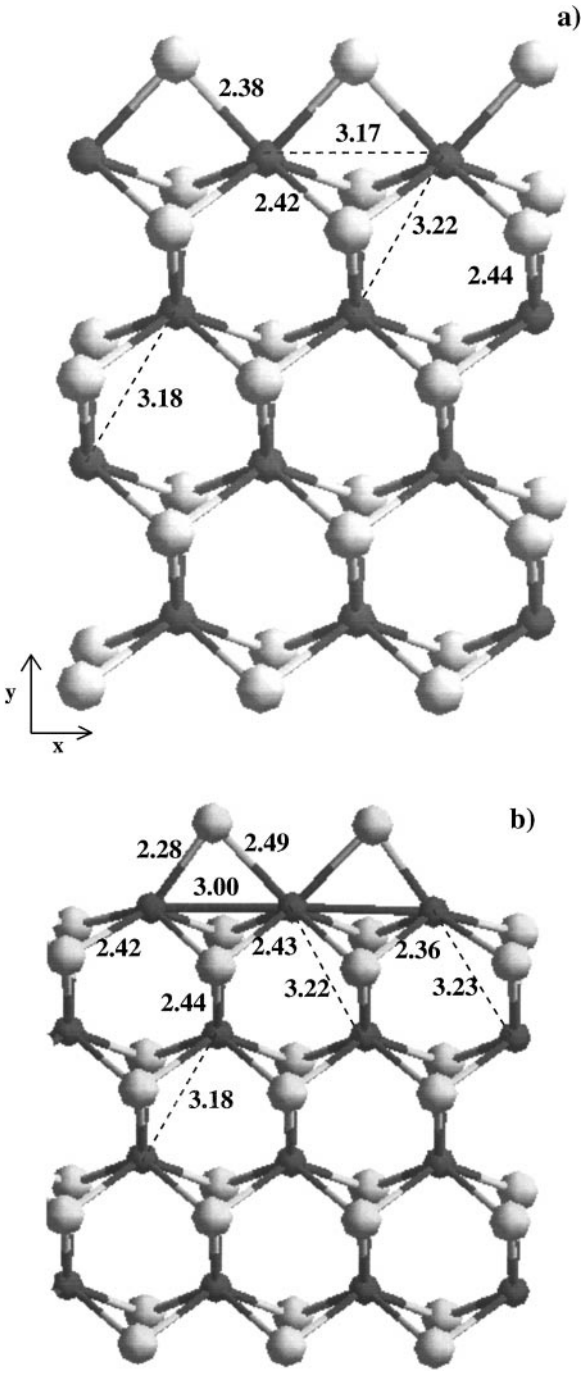

FIG. 9. Side view of the optimized structures of the Mo-terminated edge of the MoS_2 slab for various sulfur coverages: (a) 50%, (b) 33% sulfur. Small black balls, Mo atoms; large gray balls, S atoms. All distances are in Å.

equal to bulk distances. The Mo–S distances close to the surface vary between 2.38 and 2.44 Å, and the average is again in agreement with EXAFS data (2.41 Å). The surface Mo–S distances are slightly smaller (2.38 Å), whereas some bulk Mo–S distances are slightly longer (2.42 to 2.44 Å), which is consistent with the lower degree of coordination of the surface sulfur atoms. At a lower sulfur coverage of 33% (Fig. 9b), the added S atoms occupy again bridging sites between the surface Mo atoms. In this case, the distance between the S atom and the fivefold coordinated Mo atom is 0.21 Å shorter than that of the sixfold coordinated Mo site, again in accordance with the principle of bond-order conservation. Indirectly, the strong Mo–S bonds at the fivefold coordinated sites lead to shorter Mo–Mo distances between the Mo atoms bridged by the added sulfur. The average Mo–Mo distances calculated for this coverage are in any case in good agreement with the EXAFS data.

Recently, Calais *et al.* (35) as well as Shido and Prins (34) have performed a very detailed analysis of the EXAFS spectra of samples that have also been characterized by transmission electron microscopy (TEM). The EXAFS analysis shows that the distances between surface and subsurface Mo atoms are slightly larger than the Mo distances in the bulk, in agreement with the present study (3.18 to 3.22 Å) and excluding models leading to reduced Mo–Mo distances near the surface. The Mo–S coordination at the surface is estimated from the EXAFS analysis to be about 5.7, in agreement with the presence of fivefold and sixfold coordinated Mo sites in our model. This EXAFS studies also conclude that an appreciable disorder is present at the MoS_2 edge surfaces. This conjecture cannot be directly tested in a supercell calculation, but the relatively low enthalpies of reaction for S addition or removal around the equilibrium coverage of 50% are certainly consistent with some fluctuations of the local S coverage. These fluctuations in coverage would also lead to fluctuations in the local Mo–Mo distances, but the important point is that the topology of the S–Mo–S sheets close to the surface would remain essentially unchanged, independent of the degree of sulfidation of the surface.

(ii) S-terminated edge surface. We have seen that the equilibrium state of the S-terminated surface is obtained for a sulfur coverage of 100 or 50%. For a 50% coverage (see Fig. 10a), the remaining three S atoms occupy again bridging positions between the Mo sites. However, the S atoms do not remain in the mirror plane of the S–Mo–S sheets, but the Mo–S bonds are tilted such as to conform as far as possible the bonding Mo–S network existing in the solid (this is most directly visible in the side view of the slab shown in Fig. 10a2. This would probably lead to an alternating left/right/left sequence, but in our model with a repeat distance of only three Mo–Mo distances along the edge, this alternating sequence is neccessary broken. Hence the differences in the Mo–Mo and Mo–S distances in the top layer are probably not so important and only their average should be related to experimental data. The important point is that the Mo–S distances at the surface vary between 2.29 and 2.32 Å and are hence shorter than the average Mo–S distances inferred from experiments. A similar conclusion holds for the distance between surface

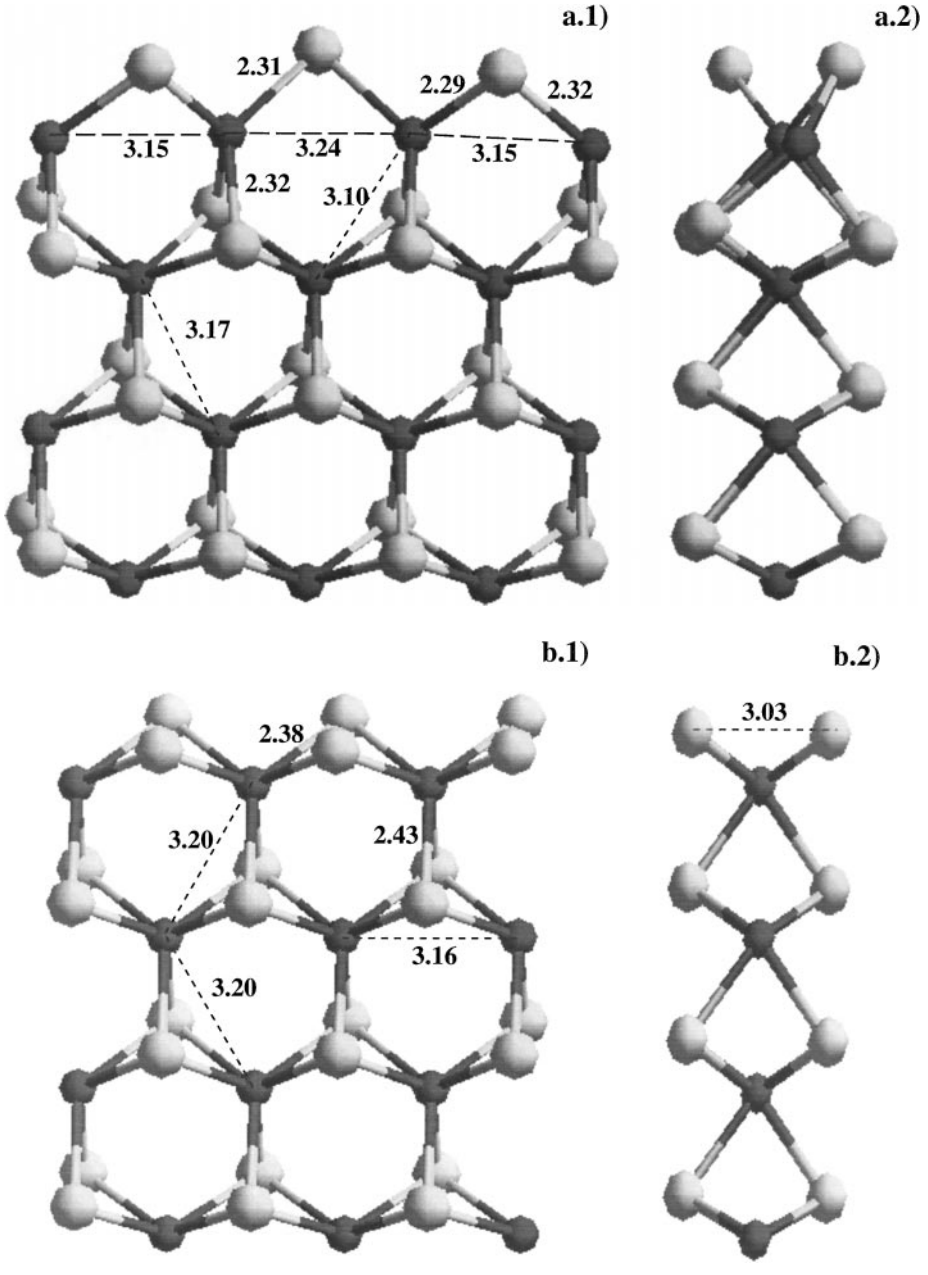

FIG. 10. Side view of the optimized structures of the S-terminated edge of the MoS_2 slab for various sulfur coverages: (a) 50%, (b) 100% sulfur. Small black balls, Mo atoms; large gray balls, S atoms. All distances are in Å.

and subsurface Mo atoms—their short distance of 3.10 Å is again distinctly below the experimental average. Also the fourfold coordination of the surface Mo atoms is distinctly below the average determined from experiment. This seems to suggest that the 50% coverage at the S edge is realized only rarely under experimental conditions and this confirms the results of the previous section showing that a 50% sulfur coverage is reached for highly reductive environment. Figure 10b shows the optimized structure of the S edge at a full coverage. As already noted (18), the fully saturated S edge undergoes only a weak relaxation, leading to a slight elongation of the distances between surface and subsurface Mo atoms over the bulk value and Mo–S distances in the top layer close to the bulk value. Both results are compatible with the EXAFS data, as is also the sixfold coordination of the Mo atoms at the edge.

Electronic Properties of Active Sites

Finally we analyze very briefly the surface electronic structure of possible active sites. We discuss first the metal sites at the Mo-terminated edge. Bulk MoS_2 is a narrow gap

semiconductor, but the coordinatively unsaturated (fourfold coordinated) Mo atoms at the bare Mo edge show a high-density of Mo–d states at the Fermi level which is directly responsible for the high reactivity of these sites (see Fig. 11) (for a detailed discussion we refer to our previous work (18)). Adsorption of S atoms causes a partial saturation of the free Mo valences and a strong modification of their electronic properties. At 33% S coverage, the density of states (DOS) is reduced on both the five- and sixfold Mo sites which bind two sulfur atoms, indicating that the donor properties of the surface Mo is more strongly reduced. On the other side, we find that there is a relatively high DOS of empty *d*-states just above the Fermi level, demonstrating that the acceptor properties of the Mo sites are less affected.

At the S-terminated edge, the DOS is given in Fig. 12 for two different sulfur coverages. At a 50% sulfur coverage, the surface Mo atoms are fourfold coordinated and exhibit a narrow gap close to the Fermi level. The occupied Mo–d states at the fermi level and at −2 eV below the Fermi level are strongly depleted, whereas the unoccupied Mo–*d* states are less affected. For a 100% sulfur coverage, only sixfold Mo atoms are present at the surface, the Mo–*d* states at the Fermi level are further depleted in comparison with the fourfold Mo sites. Even if a small acceptor peak remains just above the Fermi level, the acceptor properties are also strongly reduced in comparison with the fourfold Mo site. This case was studied in detail in previous works (18, 19)), where it was clearly shown that the sixfold Mo sites are not active regarding to the adsorption of thiophene.

DISCUSSION AND CONCLUSION

We have presented a detailed local-density–functional study of the catalytically active edge surfaces of MoS_2 under sulfiding conditions. We have shown that for an MoS_2 surface in contact with a reactive H_2/H_2S atmosphere, the dissociative adsorption of H_2S on the Mo-terminated edges of the S–Mo–S sheets and the formation of H_2 is an exothermic process up to a coverage of 50% S (i.e., one S atom adsorbed per Mo surface atom). On the S-terminated edge, the desorption of S and the reaction of the desorbing atom with H_2 to form H_2S is always an endothermic process. However, the reaction enthalpies are modest as long as the S coverage remains larger than 50%. Assuming that the desorption of S from one sheet and adsorption on the other sheet are independent processes, we can directly estimate the enthalpy for S exchange between the Mo- and S-terminated edges (the validity of this assumption has been checked by performing total energy calculations). For a stoichiometric slab, we find that the energetically most favorable distribution is 50/50 coverage of both edges. Further addition of S is a moderately exothermic process leading to an increase of the S coverage on the S-terminated edge only.

We have also analyzed the stability of different sulfur coverages as a function of the chemical potential above the surface of the catalyst. This analysis confirms that under the usual conditions in an HDS reactor, the S coverage will be around 50% on the Mo-terminated edge and around 100% on the S-terminated edge when the stacking of the catalyst particle allows the (010) surface to be fully developed along the (001) direction. However, it is likely that either 50% covered Mo edges or 100% covered S edges will appear in single sheet morphologies of the highly dispersed alumina supported industrial catalysts. This would lead to triangular shapes exhibiting either the Mo edges or the S edges, according to the working conditions. Hexagonal shapes would be observed for conditions close to the Mo-edge/S-edge transition line. In order to determine more precisely this transition we will have to compute independently the surface energies of the S edge and Mo edge in future work.

All total energy calculations underlying the preceding estimates of reaction enthalpies are based on a full structural optimization of the MoS_2 surface performed for a large model consisting of two S–Mo–S sheets, each with a thickness of four Mo–S bilayers perpendicular to the surface and extending three Mo–Mo distances along the edge. Altogether the stoichiometric model contains 72 Mo and S atoms. We find that at all coverages and in all possible configurations, the underlying MoS_2 structure undergoes only modest relaxations. The Mo–S and Mo–Mo distances close to the surface have been compared with existing EXAFS data and for the thermodynamically stable configurations, good agreement with experiment has been found. For the energetically most favorable surface with a 50% S coverage on the Mo-terminated edge, we find that S atoms adsorbed on the Mo edge are out of registry with the S atoms on the basal surface of the S–Mo–S sheets, being located in bridging positions between two surface Mo atoms (see Fig. 9a). These S atoms protrude from the edge of the S–Mo–S stacks and should be observable in an atomically resolved scanning tunneling microscopy experiment.

The fact that the MoS_2-edge surface does not reconstruct even under sulfiding conditions confirms and extends our earlier study of the stoichiometric surface (18), but is in contrast to a recent study by Byskov *et al.* (36) reporting massive reconstructions of the MoS_2 edge surface (with short Mo–Mo distances of 2.85 Å). The difference between both studies is in the size of the model: Byskov *et al.* use essentially a one-dimensional chain-like model consisting of only one S–Mo–S sheet measuring two Mo–S bilayers in depth (12 Mo and S atoms altogether for the stoichemetric slab). We have repeated some of the calculations with their setup and reconfirm their results. Hence the massive reconstruction is a consequence of the insufficient size of the model.

We have also performed a brief analysis of the electronic properties of the surfaces. We find that the adsorption of

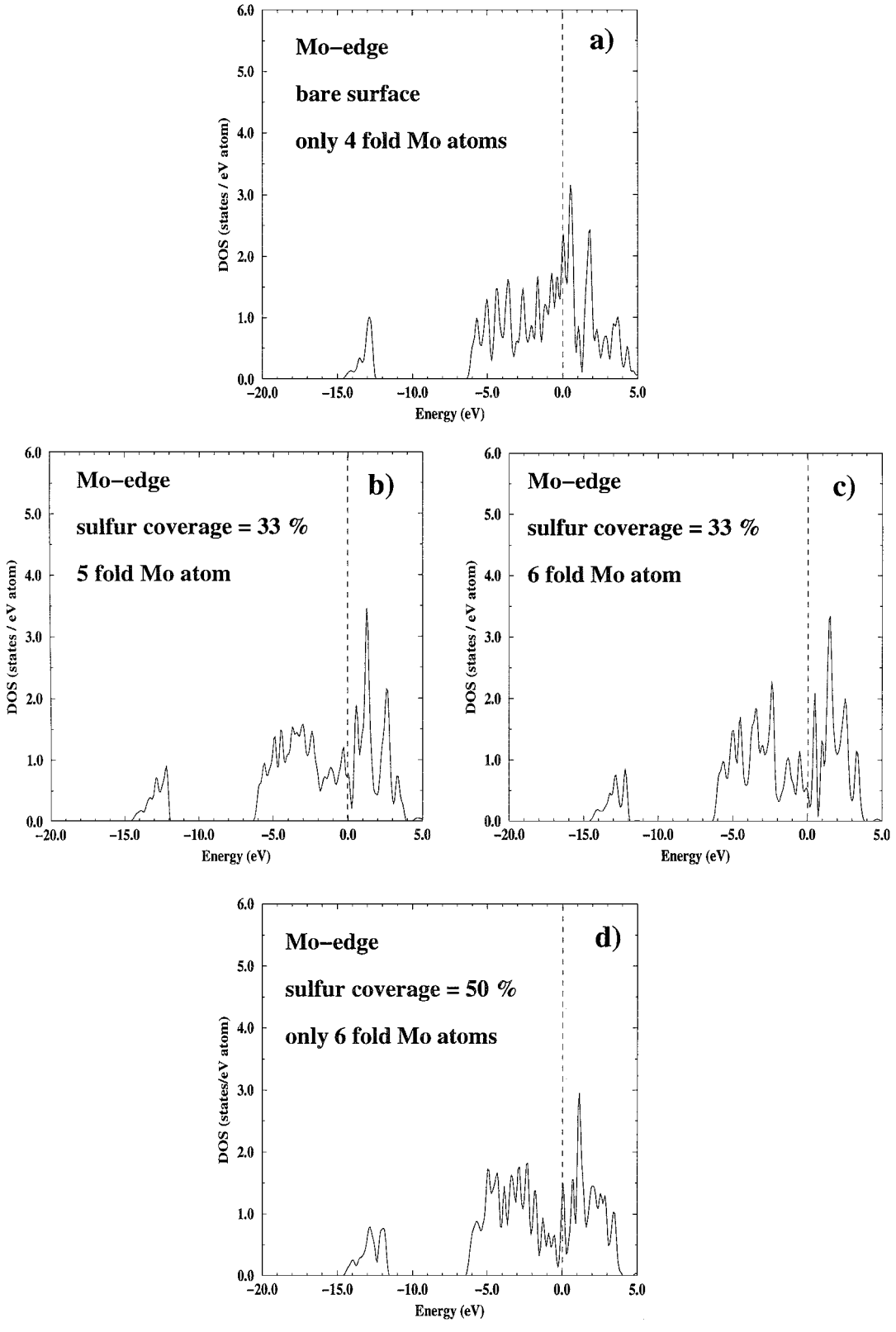

FIG. 11. Local density of states projected on the Mo surface atoms of the Mo edge for different sulfur coverages: (a) 0%, (b) 33%, (c) 50%.

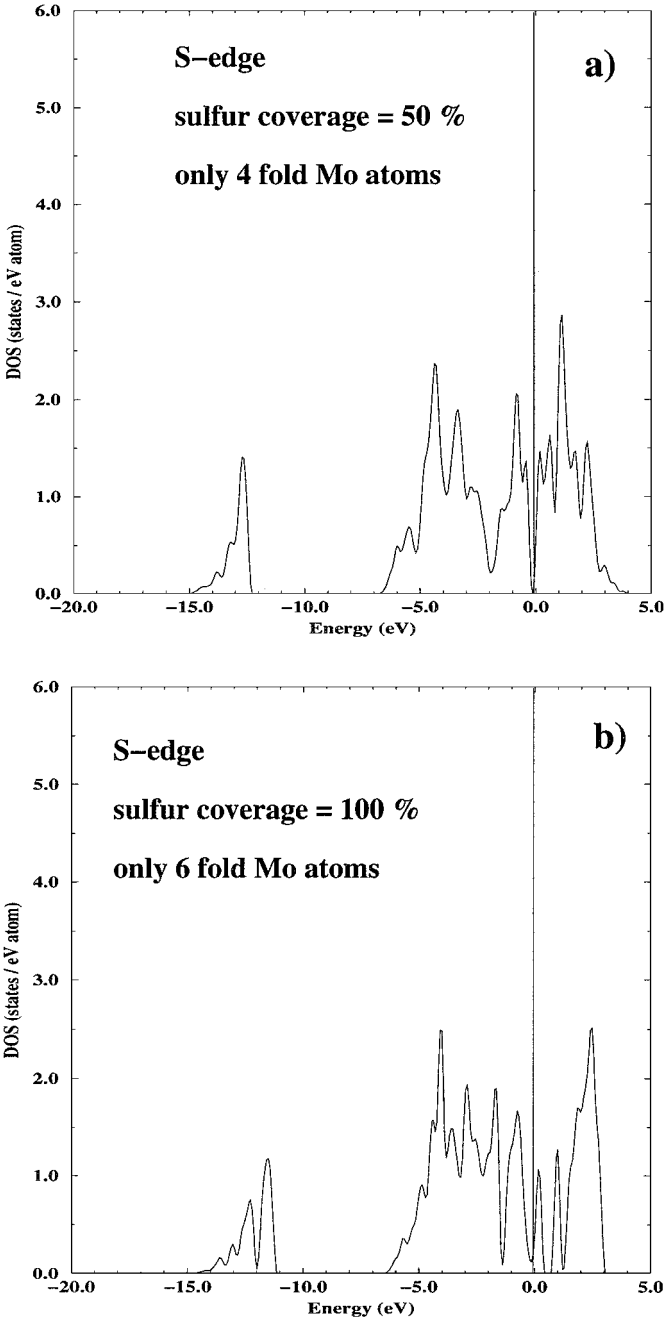

FIG. 12. Local density of states projected on the Mo surface atoms of the S edge for different sulfur coverages: (a) 50%, (b) 100%.

S on the Mo site leads to a reduction of the local Mo–4*d* DOS at the surface which is more pronounced with increasing S coordination of the Mo-edge atom. The reduced DOS of occupied states just below the Fermi energy reduces the potential donor properties of the MoS_2 surface. However, there is still an appreciable DOS of empty states just above the Fermi energy, so that acceptor properties will be less affected. Fourfold Mo atoms exhibit the strongest reactivities in terms of high DOS close to the Fermi level.

In conclusion, the results presented in this study constitute the first complete information on the stability, structure, and electronic properties of reactive MoS_2 surfaces under HDS conditions. Although we are aware of the requirement to complete this work by testing the influence of the presence of adsorbed hydrogen species (Mo–SH or Mo–H) on the sulfur coverage as well as adsorbed carbon (38) species, our results already provide the basis for a microscopic modeling of HDS reactions. Further investigations will also be directed toward the understanding of promoter effects associated with a partial substitution of surface Mo by Co or Ni.

ACKNOWLEDGMENTS

This work has been performed within the Groupement de Recherche Européen "Dynamique Moléculaire Quantique Appliquée à la Catalyse," a joint project of the Conseil National de la Recherche Scientifique (CNRS), Institut Français du Pétrole (IFP), TOTALFINA, Universität Wien, and Schuit Institute of Catalysis. Work at Universität Wien has been supported by the Institut Français du Pétrole (IFP) and by the Bundesministerium für Wissenschaft und Verkehr through the Center for Computational Materials Science (CMS).

REFERENCES

1. Delannay, F., *Appl. Catal.* **16**, 135 (1985).
2. Payen, E., Kasztelan, S., Houssenbay, S., Szymanski, R., and Grimblot, J., *J. Phys. Chem.* **93**, 6501 (1989).
3. Alstrup, I., Chorkendorff, I., Candia, R., Clausen, B. S., and Topsoe, H., *J. Catal.* **77**, 397 (1982).
4. Kasztelan, S., Grimblot, J., Bonnelle, J. P., Payen, E., Toulhoat, H., and Jacquin, Y., *Appl. Catal.* **7**, 91 (1983).
5. Clausen, B. S., Topsoe, H., Candia, R., Villadsen, J., Lengeler, B., Als-Nielsen, J., and Christensen, F., *J. Phys. Chem.* **85**, 3868 (1981).
6. Clausen, B. S., and Topsoe, H., *Hyperfine Interact.* **47**, 203 (1989).
7. Clausen, B. S., and Topsoe, H., *Catal. Rev.* **26**, 416 (1990).
8. Bouwens, S. M. A. M., Prins, R., de Beer, V. H. J., and Koningsberger, D. C., *J. Phys. Chem.* **94**, 3711 (1990).
9. Kastelan, S., Toulhoat, H., Grimblot, J., and Bonnelle, J. P., *Appl. Catal.* **13**, 127 (1984).
10. Kasztelan, S., *Langmuir* **6**, 590 (1990).
11. Harris, S., and Chianelli, R. R., *J. Catal.* **86**, 400 (1984).
12. Harris, S., and Chianelli, R. R., *J. Catal.* **98**, 17 (1986).
13. Zonnevylle, M. C., Hoffman, R., and Harris, S., *Surf. Sci.* **199**, 320 (1988).
14. Drew, M. G. B., Mitchell, P. C. H., and Kasztelan, S., *J. Chem. Soc. Faraday Trans.* **86**, 697 (1990).
15. Raybaud, P., Hafner, J., Kresse, G., and Toulhoat, H., *J. Phys. Condens. Matter* **9**, 11085 (1997); *J. Phys.: Condens. Matter* **9**, 11107 (1997).
16. Toulhoat, H., Raybaud, P., Kasztelan, S., Kresse, G., and Hafner, J., *Catal. Today* **50**, 629 (1999).
17. Byskov, L. S., Hammer, B., Norskov, J. K., Clausen, B. S., and Topsoe, H., *Catal. Lett.* **47**, 177 (1997).
18. Raybaud, P., Hafner, J., Kresse, G., and Toulhoat, H., *Surf. Sci.* **407**, 237 (1998).
19. Raybaud, P., Hafner, J., Kresse, G., and Toulhoat, H., *Phys. Rev. Lett.* **80**, 1481 (1998).
20. Kasztelan, S., Jalowiecki, L., Wambeke, A., Grimblot, J., and Bonnelle, J. P., *Bull. Soc. Chim. Belg.* **96**, 1003 (1987).

21. Wambecke, A., Jalowiecki, L., Kasztelan, S., Grimblot, J., and Bonnelle, J. P., *J. Catal.* **109**, 320 (1988).
22. Perdew, J. P., and Zunger, A., *Phys. Rev. B* **23**, 5084 (1987).
23. Perdew, J. P., Chevary, J. A., Vosko, S. H., Jackson, K. A., Pedersen, M. R., Singh, D. J., and Frolhais, C., *Phys. Rev. B* **46**, 6671 (1992).
24. Vanderbilt, D., *Phys. Rev. B* **41**, 7892 (1990).
25. Kresse, G., and Hafner, J., *Phys. Rev. B* **49**, 14251 (1994).
26. Kresse, G., and Hafner, J., *J. Phys. Condens. Matter* **6**, 8245 (1994).
27. Kresse, G., and Hafner, J., *Phys. Rev. B* **47** 588, 14251 (1993).
28. Kresse, G., and Furthmüller, J., *Computat. Mat. Sci.* **6**, 15 (1996); *Phys. Rev. B* **54**, 11961 (1996).
29. Bronsema, K. D., de Boer, J. L., and Jellinek, F., *Z. Anorg. Allgem. Chem*. **540**, 15 (1986).
30. Quian, G. X., Martin, R. M., and Chadi, D. J., *Phys. Rev. B* **38** 11, 7649 (1988).
31. Yamauchi, J., Tsukada, M., Watanabe, S., and Sugino, O., *Phys. Rev. B* **54** 8, 5586 (1996).
32. Kadas, K., Kern, G., and Hafner, J., *Phys. Rev. B* **58** 23, 1 (1998).
33. Wang, X.-G., Weiss, W., Shaikhutdinov, Sh. K., Ritter, M., Petersen, M., Wagner, F., Schlögl, R., and Scheffler, M., *Phys. Rev. Lett.* **81**, 1038 (1999).
34. Shido, T., and Prins, R., *J. Phys. Chem*. **102**, 8426 (1998).
35. Calais, C., Matsubayashi, N., Geantet, C., Yoshimura, Y., Shinada, H., Nishijima, A., Lacroix, M., and Breysse, M., *J. Catal.* **174**, 130 (1998).
36. Byskov, L. S., Norskov, J. K., Clausen, B. S., and Topsoe, H., "Preprints Symposia, Division of Petroleum Chemistry." ACS, Dallas, 1998.
37. "Handbook of Chemistry and Physics," 76th ed. 1995–1996.
38. Berhault, G., Chianelli, "Communication of the 16th Meeting of the North American Catalysis Society." Boston, 1999.
39. Besenbacher, F., "Talk at Catalysis from First Principles," Magleås, May 17–19, 1999; Topsoe, H., "Plenary talk at the 16th Meeting of the North American Catalysis Society," Boston, May 30–June 4, 1999.